Materials Today Bio 22 (2023) 100735

Contents lists available at ScienceDirect

Materials Today Bio

journal homepage: www.journals.elsevier.com/materials-today-bio

Hydrogel platform facilitating astrocytic differentiation through cell mechanosensing and YAP-mediated transcription

Zhongqian Liu [a,b], Shijie Mao [a,b], Yubin Hu [b], Feng Liu [a], Xiaowei Shao [a,b,*]

[a] School of Life Sciences, Shandong University, Qingdao, Shandong, 266237, China
[b] Institute of Marine Science and Technology, Shandong University, Qingdao, Shandong, 266237, China

ARTICLE INFO

Keywords:
Hydrogel
Neural stem cell
Astrocyte
Mechanobiology
YAP
Ca^{2+} channel

ABSTRACT

Astrocytes are multifunctional glial cells that are essential for brain functioning. Most existing methods to induce astrocytes from stem cells are inefficient, requiring couples of weeks. Here, we designed an alginate hydrogel-based method to realize high-efficiency astrocytic differentiation from human neural stem cells. Comparing to the conventional tissue culture materials, the hydrogel drastically promoted astrocytic differentiation within three days. We investigated the regulatory mechanism underlying the enhanced differentiation, and found that the stretch-activated ion channels and Yes-associated protein (YAP), a mechanosensitive transcription coactivator, were both indispensable. In particular, the Piezo1 Ca^{2+} channel, but not transient receptor potential vanilloid 4 (TRPV4) channel, was necessary for promoting the astrocytic differentiation. The stretch-activated channels regulated the nuclear localization of YAP, and inhibition of the channels down-regulated the expression of *YAP* as well as its target genes. When blocking the YAP/TEAD-mediated transcription, astrocytic differentiation on the hydrogel significantly declined. Interestingly, cells on the hydrogel showed a remarkable filamentous actin assembly together with YAP nuclear translocation during the differentiation, while a progressive gel rupture at the cell-hydrogel interface along with a change in the gel elasticity was detected. These findings suggest that spontaneous decrosslinking of the hydrogel alters its mechanical properties, delivering mechanical stimuli to the cells. These mechanical signals activate the Piezo1 Ca^{2+} channel, facilitate YAP nuclear transcription via actomyosin cytoskeleton, and eventually provoke the astrocytic differentiation. While offering an efficient approach to obtain astrocytes, our work provides novel insights into the mechanism of astrocytic development through mechanical regulation.

1. Introduction

Astrocytes are a type of glial cell that tile the entire central nervous system (CNS) and are essential for brain homeostasis. They provide physical and metabolic supports for neurons, coordinate synapse formation and functions, comprise the blood-brain barrier, and respond to injuries and diseases [1,2]. As the diversity of astrocyte functions increases, it is extremely helpful to establish *in vitro* platforms to study the human-specific astrocytes in the context of physiology and diseases [2,3]. One way to obtain human astrocytes is by inducing neural stem cell (NSC) differentiation, as shown in several previous studies [4–6]. However, the currently available methods are usually complex and time-consuming. Therefore, an efficient approach to obtain human astrocytes is highly desired.

Mechanical signals, such as matrix elasticity, regulate NSC differentiation into astrocytes. While compliant substrates with elastic modulus <1 kPa preferably direct NSCs into neuronal cells, relatively stiffer substrates (1–10 kPa) preferably lead to astrocytes and oligodendrocytes [7,8]. A study using human NSCs (hNSCs) has demonstrated that the stretch-activated Ca^{2+} channel, Piezo1, promotes neurogenesis and suppresses astrogenesis, possibly via Yes-associated protein (YAP) [9]. In contrast, evidence in the rodents shows that YAP promotes astrocytic differentiation through Smad1, downstream of bone morphogenetic protein (BMP) signaling [10,11]. Also in rodents, YAP has been identified to negatively regulate neuronal differentiation by sensing the rigidity [12,13]. Therefore, how mechanical cues, Ca^{2+} channels, and YAP transcription coactivator synergize to regulate the astrocytic differentiation from NSCs remains to be further clarified.

Alginate is a biocompatible and easily available marine polysaccharide extracted from brown algae, which can be divalently

* Corresponding author. School of Life Sciences, Shandong University, Qingdao, Shandong, 266237, China.
E-mail address: shaoxw@email.sdu.edu.cn (X. Shao).

https://doi.org/10.1016/j.mtbio.2023.100735
Received 24 March 2023; Received in revised form 29 June 2023; Accepted 19 July 2023
Available online 20 July 2023

crosslinked to form hydrogels of tunable mechanical properties [14,15]. In this study, we employed an alginate hydrogel-based matrix, prepared using a thaw-induced, Ca^{2+}-crosslinked gelation method. We found that the astrocytic differentiation of hNSCs was drastically enhanced on the hydrogel, comparing to that on the conventional tissue culture polystyrene (PS). Mechanistically, the mechanosensitive Ca^{2+} channels and YAP-mediated transcription were both necessary for the differentiation: Firstly, cells grown on the hydrogel showed significantly higher intracellular Ca^{2+} level comparing to those on the PS; inhibition of mechanosensitive ion channels during the differentiation successfully brought down the intracellular Ca^{2+} level and attenuated the astrocyte development. Secondly, using chemical inhibitors and agonists, we found that the transient receptor potential vanilloid 4 (TRPV4) mechanosensitive channel was dispensable, while Piezo1 was essential, for the enhanced on-gel astrocytic differentiation. Further, the nuclear localization of YAP was found to be affected by the stretch-activated channels, and blocking the YAP/transcriptional enhanced associate domain (TEAD)-mediated transcription led to declined astrocytic development on the hydrogel. Finally, cells on the hydrogel showed a remarkable filamentous actin (F-actin) reinforcement together with YAP nuclear translocation during the differentiation, and at the meantime, a progressive gel rupture at the cell-hydrogel interface along with a change in the gel elasticity were detected. With these findings, we elucidate the mechanotransduction mechanism underlying the on-gel astrocytic development, in which mechanical stimuli delivered by the gel decrosslinking give rise to activation of Piezo1 Ca^{2+} channel and further the YAP-mediated transcription, resulting in high-efficiency astrocytic differentiation.

2. Materials and methods

2.1. Preparation of alginate hydrogel

Sodium alginate (Sigma-Aldrich) was dissolved in Milli-Q water at 70 °C to make a 1.5%–3.5% (w/v) aqueous solution. The cross-linking solution contains 90 mM $CaCl_2$ and 150 mM NaCl. Both solutions were sterilized with a 0.22 μm filter. Alginate hydrogels were prepared using a thaw-induced gelation method [16]. In brief, the sodium alginate solution was added to the culture plate at 45 μl/cm^2 and kept at −80 °C for 15 min to freeze. Then, the cross-linking solution was quickly added to the frozen sodium alginate at 250 μl/cm^2. The mixture was kept at room temperature for 2.5 h to allow the gelation to occur. After removing the excess liquid, followed by brief washing, the hydrogel was coated with 20 μg/ml laminin derived from Engelbreth-Holm-Swarm mouse sarcoma basement membrane (Sigma-Aldrich, L2020) in phosphate-buffered saline (PBS) buffer containing Ca^{2+} and Mg^{2+} and incubated at 37 °C overnight.

2.2. Rheology, scanning electron microscopy (SEM), and atomic force microscopy (AFM)

Rheological characterization of hydrogels was performed using a Discovery HR-3 rheometer (TA Instruments, Waters). All samples were made into a circular-shaped thin layer, about 60 mm in diameter and 1–2 mm thick. The elastic modulus and viscous modulus measurements of hydrogels were carried out at an angular frequency of 10 rad/s at 37 °C. For SEM, the cells were first fixed with 2.5% glutaraldehyde for 30 min at 4 °C, and then the hydrogel was dehydrated by gradient ethanol series (30%, 50%, 70%, 90%, and 100%) followed by lyophilization. After coated with gold for 1 min, the samples were examined on a Quattro environmental SEM (Thermo Scientific). The AFM characterization was done on JPK Nanowizard4. Briefly, a pyramidal probe with spring constant 1.013 N/m was used to scan the surface of the hydrogel in quantitative imaging mode. JPK Data Processing software was used to fit the curves and analyze the data. The Hertz model was used to determine the elastic modulus maps with a sample Poisson ratio of 0.5 fitting over a range of 10–90% indentation force.

2.3. Cell culture, differentiation, and drug treatment

ReNcell VM hNSCs were purchased from Millipore. Cells were plated on laminin-coated tissue culture plates or alginate hydrogel and maintained in DMEM/F-12 medium (Gibco) containing 10 u/ml heparin (Sigma-Aldrich), 2% (v/v) B27 neural supplement (Gibco), 20 ng/ml epidermal growth factor (EGF) (PeproTech), 20 ng/ml basic fibroblast growth factor (FGF2) (PeproTech), and 1% (v/v) Antibiotic-Antimycotic (Gibco) at 37 °C in a cell culture incubator with 5% CO_2. For astrocyte induction, hNSCs were seeded at a density of 25,000 cells/cm^2. The next day, EGF and FGF2 were withdrawn from the maintenance medium, and 5% (v/v) fetal bovine serum (FBS) was added. The astrocytic differentiation lasted 3 days. $GdCl_3$ (Sigma-Aldrich) was used to inhibit the mechanosensitive ion channels, and 100 μM $GdCl_3$ was added into the astrocytic differentiation medium 24 h after the differentiation started, and the treatment lasted another 24 h. The Ca^{2+} signals and YAP localizations were analyzed once the treatment was completed, and the astrocytic lineage markers were analyzed after the differentiation was completed. For TRPV4 channel inhibition, the cells were treated with 1 μM GSK2193874 (Sigma-Aldrich) during the differentiation. To inhibit the Piezo channels, 5% FBS was replaced by 100 ng/ml BMP2 to induce astrocytic differentiation. The cells were treated with 5 μM GsMTx4 (MedChemExpress) during the differentiation. Yoda1 (Sigma-Aldrich) was used to provoke Piezo1 activation at a concentration of 50 μM during the differentiation. Verteporfin (Sigma-Aldrich) was used to inhibit the YAP/TEAD-mediated transcription at a concentration of 0.5 μg/ml during the astrocytic differentiation. Cytochalasin D (Sigma-Aldrich) was used to inhibit actin polymerization at a concentration of 5 μM. Blebbistatin (Sigma-Aldrich) was used to inhibit non-muscle myosin II at a concentration of 50 μM during the differentiation.

2.4. Immunofluorescence, microscopy, and imaging analyses

The live cells were stained by CFSE (Abcam) dissolved in the culture medium for 15 min at 37 °C. For immunofluorescence, cells were fixed with 4% paraformaldehyde in PBS for 20 min and permeabilized with 0.2% Triton X-100 for 10 min. Cells were then blocked with 3% bovine serum albumin in PBS for 1 h, followed by primary and secondary antibody staining for 1 h each at room temperature. The PBS buffer used in all steps of immunofluorescence contains Ca^{2+} and Mg^{2+} to avoid alginate gel degradation. The primary antibodies used were: anti-Nestin (ab6320, Abcam), anti-Sox2 (ab97959, Abcam), anti-Ki67 (ab8191, Abcam), anti-GFAP (130300, Invitrogen), anti-S100B (ab52642, Abcam), anti-YAP (sc101199, Santa Cruz). F-actin was stained by Rhodamine-conjugated phalloidin for 30 min. Microscopy images were mainly acquired on Nikon Ti2 fluorescence microscope. The images with Z-stacks were acquired on Zeiss LSM880 confocal microscope.

The fluorescence images were processed and analyzed by Image J after subtracting background fluorescence. To quantify the cellular fluorescence of a marker under a certain condition, fluorescence images were captured at a focal plane where the cells were found brightest. The total projected fluorescence of an imaging field was calculated and then divided by the number of nuclei, resulting in an averaged “total cellular fluorescence intensity”, and in short “Fluo. Int”. Unless otherwise specified, quantifications on “Fluo. Int” were made on imaging fields (shown as dots on the graphs), which were captured under the same microscopy settings from 3 to 4 independent experiments (i.e., biological repeats). To quantify the YAP nuclear-to-cytoplasmic ratios, the nuclei were identified by Hoechst staining, which were used as the regions of interest (ROI) to segment the nuclear and cytoplasmic proportions. Based on the total YAP fluorescence per imaging field, the nuclear-to-cytoplasmic ratios were calculated. More details including statistical information are provided in the legend of each figure.

2.5. Hydrogel digestion, quantitative PCR (qPCR), and western blot

To harvest the cells grown on the alginate hydrogel, the culture was incubated in a PSB buffer (without Ca^{2+}/Mg^{2+}) containing 20 mM EDTA and 55 mM sodium citrate for 15–20 min to digest the gel. Cells were then harvested and lysed, and total RNA was extracted using Quick-RNA™ Microprep Kit (ZYMO) following the manufacturer's instructions. The reverse transcription was conducted using PrimeScript™ RT reagent Kit with gDNA Eraser (TaKaRa). LightCycler® 480 SYBR Green I Master (Roche) was used for the amplification and detection of cDNA targets on a CFX Connect system (Bio-Rad). The relative mRNA levels of target genes were analyzed using $2^{-\Delta Ct}$, normalized to the level of the housekeeping gene *GAPDH*. The primers for qPCR are as follows: *GAPDH* (forward-tgcaccaccaactgcttagc, reverse-ggcatggactgtggtcatgag); *GFAP* (forward-gaagctccaggatgaaacca, reverse-acctcctcctcgtggatctt); *S100B* (forward-tggccctcatcgacgttttc, reverse-atgttcaaagaactcgtggca); *NESTIN* (forward-ctgctacccttgagacacctg, reverse-gggctctgatctctgcatctac); *SOX2* (forward-gccgagtggaaacttttgtcg, reverse-ggcagcgtgtaaccatcctt ct); *NANOG* (forward-aaggtcccggtcaagaaacag, reverse-cttctgcgtcacaccat tgc); *OCT4* (forward-gagtgagaggcaacctggag, reverse-gccggttacagaacc acact); *DCX* (forward-gacagcccactcttttgagc, reverse-tgggtttcccttcatga ctc); *YAP* (forward-tttctcctgggacactgacc, reverse-tctttgccatctcccaacct); *ANKRD1* (forward-agtagaggaactggtcactgg, reverse-tgggctagaagtgtcttca gat); *CYR61* (forward-ggaaaaggcagctcactgaagc, reverse-ggagataccagttc cacaggtc); *CCND1* (forward-gcatgttcgtggcctctaag, reverse-ttcaatgaaatcg tgcgggg).

For western blot, cells were harvested and then lysed in 2x Laemmli Sample Buffer. After heating for 10 min at 95 °C, the protein extracts were separated by SDS-PAGE and transferred to PVDF membranes (MerckMillipore). After blocking with 5% skim milk in TBST for 1 h, the membranes were incubated with primary antibodies overnight at 4 °C. After washing, the membranes were incubated with HRP-conjugated secondary antibodies. Bound antibodies were detected by HRP Chemiluminescent Reagent (Merck) and Tanon 5200 Chemiluminescent Imaging System. The primary antibodies used in the western blot were anti-GFAP (130300, Invitrogen), anti-S100β (ab52642, Abcam), and anti-α-Tubulin (ab176560, Abcam). Secondary antibodies were HRP-conjugated anti-rat IgG (31470, Invitrogen) and anti-rabbit IgG (31466, Invitrogen).

2.6. Ca^{2+} measurements

Intracellular Ca^{2+} level was indicated by a fluorescent Ca^{2+} indicator, Fluo-4, AM (F14201, ThermoFisher), following the manufacturer's instructions. Fluorescence images were recorded every 3 s. The spontaneous Ca^{2+} transients in the cells were shown by $\Delta F/F$, where ΔF is the amplitude of the Ca^{2+} fluorescence signal, i.e., F_{max}-F_{min}, and F is the average Ca^{2+} fluorescence signal at the steady state. Ca^{2+} concentration in the tissue culture supernatant was determined using an automatic potentiometric titrator (T960, Hanon). Sodium tetraborate buffer was used to adjust pH, and EGTA was used as a titrant. The end point of titration was determined using the second-order derivative method.

2.7. Statistical analyses

All the data with error bars are presented as Mean ± Standard Error (SE). GraphPad software was used for plotting graphs and for statistical analyses. Unless otherwise stated, statistical significance was tested by two-tailed student's *t*-test (*$p < 0.05$, **$p < 0.01$, ***$p < 0.001$, ****$p < 0.0001$) when comparing the difference between two samples.

3. Results

3.1. The hydrogel substrate drastically promotes astrocytic differentiation

To mimic the mechanical microenvironment of brain tissues, a soft substrate made of alginate hydrogel was exploited, in which Ca^{2+} was used as the crosslinker of alginate. However, direct mixing of the sodium alginate and Ca^{2+} solutions led to immediate gelation that generated uneven gel surface, unsuitable for tissue culture and *in-situ* observation. Hence, we developed a thaw-induced gelation method to prepare the hydrogel by adding $CaCl_2$ solution to the frozen alginate. In this way, the Ca^{2+} crosslinking occurred slowly while the alginate solution was thawed (Fig. 1A-left, see Materials and Methods for details), resulting in a smooth and homogeneous hydrogel surface (Fig. 1B-left). Using 1.5%–3.5% sodium alginate and 90 mM $CaCl_2$ aqueous solutions, hydrogels with different surface porosity, elastic and viscous modulus were obtained, as characterized by SEM (Fig. 1C) and oscillatory rheology (Fig. 1D). The elastic modulus (G′) of the hydrogel was shown to increase with the concentration of sodium alginate, in the range of 0.03–3.06 kPa, comparable to the elasticity of native brain tissues (0.1–1 kPa) measured using the same tool [17,18] (Fig. S1). A time lag (or phase shift, δ) between the oscillating stress and the corresponding periodic material deformation was observed, where $0 < \delta < \pi/2$, characterizing the hydrogels as viscoelastic materials. Since G′ was higher than G'' (i.e., $\delta < \pi/4$) (Fig. 1D), these gels were mainly elastic [19].

Upon coating with laminin, the hNSCs could grow healthily on the hydrogel (Fig. 1A-right), which showed excellent viability, as revealed by live cell staining using CFSE (Fig. 1E), and expressed NSC markers Nestin and Sox2 (Fig. 1F). Comparing to those on PS, hNSCs grown on the hydrogel displayed a more neural-like morphology, i.e., slim, elongated, and smaller in size (Fig. 1B-right, Fig. 1E-bright field images, Fig. 1G). The smaller cell area on the hydrogel can be attributed to the lower rigidity of hydrogel, as the spreading area is dictated mechanically by a force-balance between the cell and the substrate involving the formation of focal adhesion and stress fibers, as reported previously [20–22]. Cells grown on the hydrogel also showed a smaller Ki67-positive percentage and a lower density (Fig. 1H), indicating a lower proliferation potential. Consistently, cells grown on the hydrogel expressed lower levels of genes on NSC stemness (*NES, SOX2, NANOG, OCT4*), and higher levels of genes on neuronal (*DCX*) and astrocytic (*S100B*) lineages, suggesting a higher differentiation potential (Fig. 1I).

To induce astrocytic differentiation, 5% FBS was added to the NSC maintenance medium without growth factors (Fig. 2A) [4]. The astrocytic lineage markers S100B and GFAP express extensively in three days according to our previous study [23]. Considering the elasticity of native brain tissues (0.1–1 kPa), 1.5%–3% hydrogels (0.03–2.18 kPa) were initially employed here, and the differentiation was found similar on those hydrogels, as indicated by GFAP immunofluorescence (Fig. 2B–C). The highest level of S100B was shown on 2.5% hydrogel (Fig. 2B–C), which was therefore used in all the subsequent experiments to represent the hydrogel. Remarkably, comparing to the PS substrate (elastic modulus in the order of GPa) [8,24], astrocytic differentiation on the alginate hydrogel was drastically enhanced, as revealed by immunofluorescence of S100B and GFAP (Fig. 2E–F, S2), and verified by immunoblots (Fig. 2G) and mRNA quantifications of those genes (Fig. 2H). Hence, we went on to investigate the mechanism leading to the robust promotion of astrocytic differentiation on the alginate hydrogel.

3.2. Mechanosensitive Ca^{2+} channels are required to promote astrocytic differentiation on the hydrogel

To figure out the mechanism underlying the enhanced astrocytic differentiation on the hydrogel, we started with examining the involvement of the stretch-activated Ca^{2+} channels, which often contribute to stem cell differentiation [9]. Using a cell-permeable Ca^{2+} indicator, Fluo-4 AM, the intracellular Ca^{2+} level on different substrates was observed (Fig. 3A). Noticeably, the cells differentiated on the alginate hydrogel showed a significantly higher Ca^{2+} level and stronger Ca^{2+} oscillations, comparing to the cells on PS (Fig. 3A–C). The lanthanide Gd^{3+} is known to inhibit the stretch-activated ion channels [25,26], which was employed in this study. When cells on the gel were

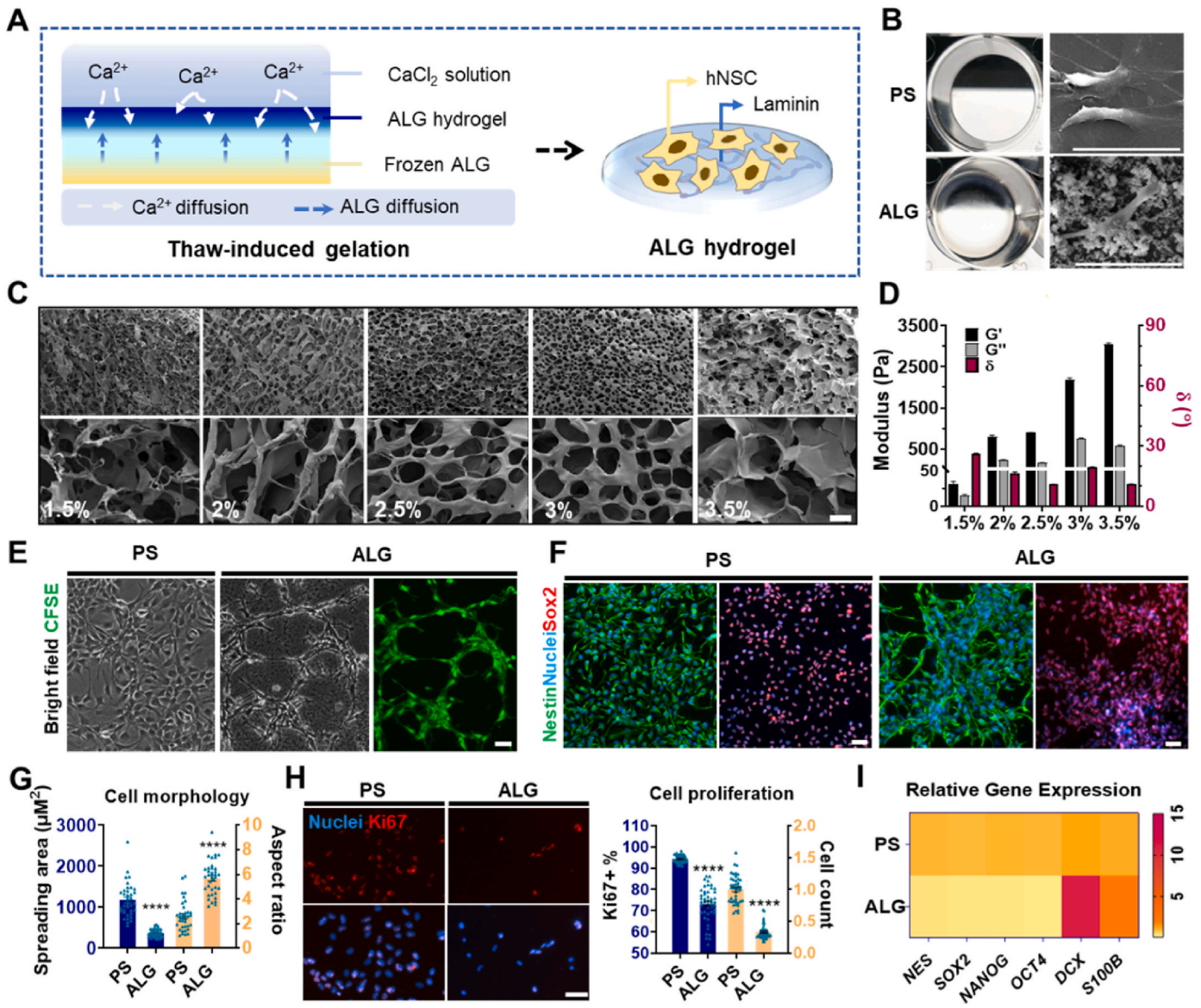

Fig. 1. Preparation and characterizations of the alginate hydrogel substrate. **(A)** Schematic of the thaw-induced gelation method to prepare alginate (ALG) hydrogel (left) and growth of hNSCs on the hydrogel (right). **(B)** (left) Photographs showing the tissue culture PS and alginate hydrogel substrates; (right) SEM images showing the cell morphology on those substrates. **(C)** SEM images showing the surface structures of the hydrogels formed by 1.5%–3.5% sodium alginate. **(D)** Oscillatory rheological measurements of the hydrogels formed by 1.5%–3.5% sodium alginate. The elastic modulus (G′), the viscous modulus (G″), and the phase shift (δ) between the oscillating stress and the periodic material deformation are shown. Measurements were performed at a constant frequency of 10 rad/s at 37 °C. **(E)** Images of hNSCs grown on PS and on 2.5% alginate hydrogel. Green fluorescence indicates CFSE that stains live cells. **(F)** Immunofluorescence of NSC marker Nestin (green) or Sox2 (red) in cells cultured on PS and on 2.5% alginate hydrogel. Images are superimposed with nuclei staining by Hoechst (blue). **(G)** Quantifications of spreading area and aspect ratio on the cells grown on PS and on 2.5% alginate hydrogel. N = 36 individual cells. **(H)** (left) Ki67 immunofluorescence in cells grown on PS and on 2.5% alginate hydrogel 24 h after seeding; (right) Percentage of Ki67-positive cells and cell count per imaging field quantified on the fluorescence images. N = 42 imaging fields from three experiments. **(I)** Relative mRNA levels of genes indicating NSC stemness or neuronal and astrocytic lineages. *GAPDH* was used as an internal control. N = 3. Data are presented as Mean ± SE. ****p < 0.0001, two-tailed student's *t*-test. (Scale bars: 50 μm). (For interpretation of the references to color in this figure legend, the reader is referred to the Web version of this article.)

treated with $GdCl_3$, the Ca^{2+} level and spontaneous Ca^{2+} oscillation declined significantly (Fig. 3D), indicating a role of stretch-activated channels in regulating cellular Ca^{2+} concentration and signaling. $GdCl_3$ treatment during the differentiation also led to significantly reduced expressions of both S100B and GFAP in cells on the hydrogel, as revealed by immunofluorescence (Fig. 3E–F), immunoblots (Fig. 3G), and mRNA quantifications (Fig. 3H). These results suggest important contributions of the stretch-activated channels and Ca^{2+} signaling to the enhanced astrocytic differentiation on the hydrogel.

Further, we asked which type of the stretch-activated channels predominantly regulated this process, and two types of the most frequently studied Ca^{2+} channels, TRPV4 and Piezo, were examined. Previous studies have demonstrated that TRPV4 can be directly activated by membrane stretching in endothelial cells and chondrocytes [27,28]. Here, we found that blocking TRPV4 activity using its inhibitor GSK2193874 did not impede astrocytic differentiation on the hydrogel, but even elevated the expression level of S100B (Fig. 4A–B), suggesting a dispensable role of TRPV4 in provoking astrogenesis. To check the contribution of Piezo1 channel, a specific agonist, Yoda1 [29], was first employed. Yoda1 treatment led to enhanced differentiation of astrocytes on the hydrogel, comparing to the nontreated condition (Fig. 4A–B). Further, an inhibitor of Piezo channels, GsMTx4, was employed [9,30].

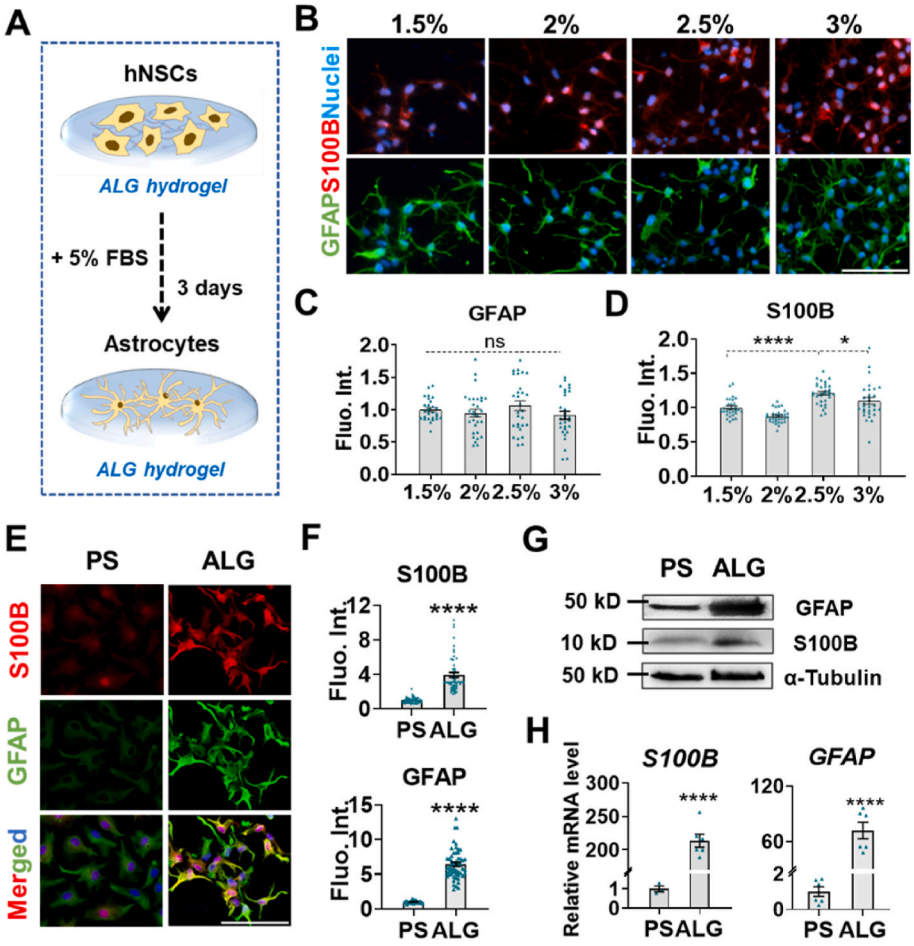

Fig. 2. Astrocytic differentiation is drastically enhanced on the hydrogel substrate. **(A)** Schematic of the astrocytic differentiation from hNSCs on the alginate hydrogel. **(B)** Induced hNSCs differentiation into astrocytes on 1.5%–3% alginate hydrogels. After 3 days of differentiation, cells were immune-stained against the astrocytic marker S100B (red) or GFAP (green). Images are superimposed with nuclei staining by Hoechst (blue). **(C–D)** Quantifications on immunofluorescence of GFAP (C) and S100B (D) on 1.5%–3% alginate hydrogels. Data are shown as averaged total cellular fluorescence intensity. N ≥ 27 imaging fields from three experiments. **(E)** Differentiation of hNSCs into astrocytes on PS substrate and on 2.5% alginate hydrogel. Immunofluorescence indicates S100B (red) and GFAP (green). Nuclei are stained by Hoechst (blue). **(F)** Quantifications on the fluorescence images showing levels of astrocytic markers after 3 days of differentiation. Data are shown as averaged total cellular fluorescence intensity. N ≥ 43 imaging fields from four independent experiments. **(G)** Immunoblots of astrocytic markers after the differentiation on PS and on hydrogel. α-Tubulin served as an internal control. **(H)** Relative mRNA levels of astrocytic marker *S100B* or *GFAP* after 3 days of astrocytic differentiation. *GAPDH* was used as an internal control. N = 6 from two independent experiments. All data are presented as Mean ± SE, normalized to the first column. Ns (not significant) $p > 0.05$, *$p < 0.05$, ****$p < 0.0001$, two-tailed student's *t*-test. (Scale bars: 100 μm). (For interpretation of the references to color in this figure legend, the reader is referred to the Web version of this article.)

Because FBS used to induce astrocytic differentiation elsewhere in this work is known to interfere with the effectiveness of GsMTx4 [31], in this particular experiment, it was replaced by BMP2, which turned out to induce astrocytic differentiation similarly to FBS [5,10] (Fig. S3). As expected, we observed that GsMTx4 treatment significantly attenuated astrocyte development on the hydrogel (Fig. 4C–D). Together, these experiments strongly suggest that Piezo1, but not TRPV4, is responsible for prompting astrocytic differentiation on the alginate hydrogel.

3.3. *YAP-mediated transcription and actomyosin cytoskeleton contributes to promoting astrocytic differentiation on the hydrogel*

Next, we went on to examine the involvement of the YAP transcription coactivator, which had been shown to promote astrocytic differentiation in rodents [10,11,32], in the context of the current study. Interestingly, when blocking the stretch-activated channels using $GdCl_3$ during the differentiation, the nuclear fraction of YAP decreased in cells on the hydrogel (Fig. 5A–B). Consistently, upon the disruption of Piezo1 channel, using either $GdCl_3$ or GsMTx4, the mRNA levels of *YAP* and the YAP/TEAD target genes *ANKRD1* and *CYR61* [33–35], dropped significantly (Fig. S4). These findings strongly indicate an upstream regulation by the mechanosensitive channel, in particular Piezo1, on YAP-mediated transcription, as reported by other studies [9,36]. To examine whether the YAP/TEAD-mediated transcription was responsible for astrocytic differentiation, verteporfin, a YAP inhibitor disrupting the YAP-TEAD interaction, was employed. Treatment of verteporfin remarkably attenuated the expression levels of the YAP/-TEAD target genes, such as *ANKRD1, CYR61*, and *CCND1* (Fig. S4), validating the effectiveness of this inhibitor. The verteporfin treatment also reduced the nuclear fraction of YAP (Fig. 5C–D), and most importantly, it significantly impeded the astrocytic differentiation on the hydrogel, indicated by both S100B and GFAP levels based on the immunofluorescence (Fig. 5E–F). This effect of verteporfin on astrocytic differentiation was further verified by qPCR mRNA measurements of *S100B* and *GFAP* genes (Fig. 5G). These results show that the YAP/TEAD-mediated transcription makes crucial contributions to the robust promotion of astrocytic differentiation on the alginate hydrogel.

The YAP nuclear localization is known to increase with the substrate rigidity, and regulated by the actomyosin cytoskeletal tension [37]. Then the question remains why the softer hydrogel unexpectedly promoted a YAP-dependent astrocyte formation here. To figure it out, we examined the F-actin structure together with YAP localization before and after the astrocytic differentiation. Consistent with the current understanding, before the differentiation, YAP exhibited a larger nuclear fraction on the (stiffer) PS than that on the (softer) hydrogel (Fig. 5H and J, "Day 0"); disrupting the actin cytoskeleton using Cytochalasin D successfully repelled the nuclear YAP (Figs. S5A–B). However, when differentiation was induced, cells on the hydrogel displayed a more significant F-actin assembly as well as nuclear migration of YAP, comparing to that on the PS (Fig. 5H and I-J, "Day3/Day0"). Cytochalasin D treatment reduced the YAP nuclear translocation on the hydrogel (Fig. S5C), and partially attenuated the astrocytic differentiation (Fig. 5K). Similarly, releasing the cytoskeletal tension using myosin II inhibitor Blebbistatin also attenuated the astrocytic differentiation (Fig. 5L). These findings indicate that actomyosin contractility indeed governed YAP nuclear translocation and astrocytic differentiation, and meanwhile, additional mechanical cues, other than rigidity, must had taken the dominant part during differentiation on the hydrogel, which

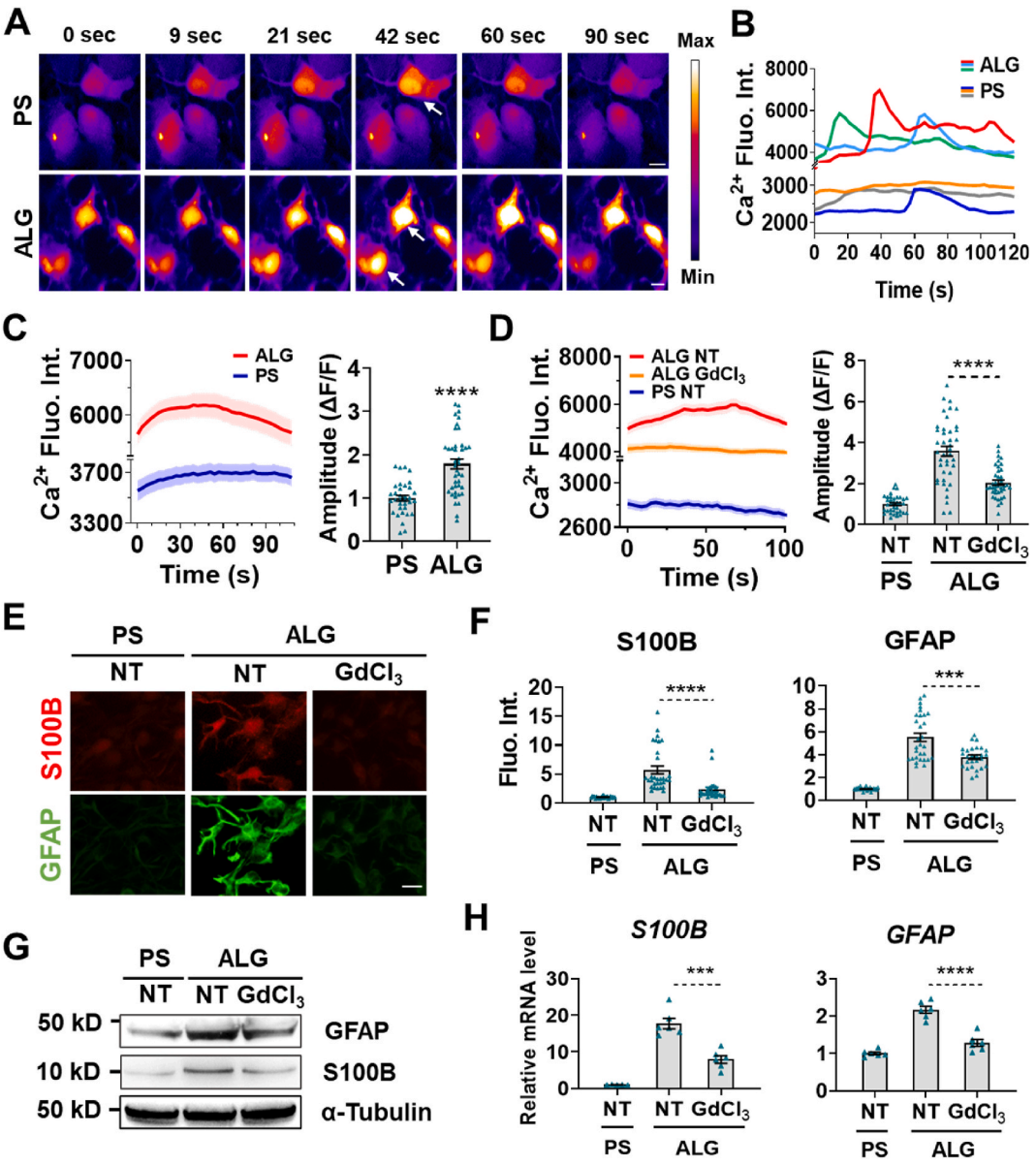

Fig. 3. Stretch-activated ion channels are required to promote astrocytic differentiation on the hydrogel. **(A)** Time-lapse images showing fluorescence intensity of Ca^{2+} indicator (Fluo-4 AM) in the cells grown on PS (upper) and on alginate hydrogel (lower) on the third day of astrocyte differentiation. The color-coded images are shown in fire scale and were prepared using Image J. Arrows indicate cells with spontaneous Ca^{2+} transients. **(B)** Examples of spontaneous Ca^{2+} transients, shown as plots of Ca^{2+} fluorescence intensity over time, in cells differentiated on PS and on alginate hydrogel. (C) (Left) Average Ca^{2+} fluorescence intensity over time, showing the spontaneous Ca^{2+} transients from multiple individual cells; and (Right) relative amplitude of the spontaneous Ca^{2+} transients, calculated as the changed fluorescence value (ΔF)/average value at steady state (F), measured from individual cells on the third day of differentiation. N ≥ 34 cells. **(D)** Effects of $GdCl_3$ to cells grown on hydrogel on intracellular Ca^{2+} signals: (Left) Average Ca^{2+} fluorescence intensity over time showing the spontaneous Ca^{2+} transients; (Right) relative amplitude of the spontaneous Ca^{2+} transients. The treatment started 24 h after initiating the differentiation and lasted for another 24 h Ca^{2+} signals were analyzed once the treatment was completed. NT indicates nontreated control. N ≥ 36 cells. **(E–F)** Immunofluorescence images (E) and quantifications (F) of astrocytic markers S100B and GFAP showing the effects of $GdCl_3$ treatment on cells on the hydrogel. Data is shown as averaged total cellular fluorescence intensity. N ≥ 24 imaging fields from three experiments. **(G)** Immunoblots of astrocytic markers showing the effects of $GdCl_3$ treatment on cells on the hydrogel. α-Tubulin served as an internal control. **(H)** Relative mRNA levels of astrocytic markers showing the effects of $GdCl_3$ on cells on the hydrogel. *GAPDH* gene was used as an internal control. N = 6 measurements. All data are presented as Mean ± SE, normalized to the first columns. NT, nontreated control. Ns, $p > 0.05$; **$p < 0.01$, ***$p < 0.001$, ****$p < 0.0001$, two-tailed student's *t*-test. (Scale bars: 10 μm). (For interpretation of the references to color in this figure legend, the reader is referred to the Web version of this article.)

led to mechanosensitive channels activation, F-actin assembly and YAP nuclear translocation.

3.4. The hydrogel substrate delivers mechanical cues to cells and promotes astrocytic differentiation

Concerning the chemical properties of the alginate hydrogel, we speculate that the spontaneous decrosslinking of the gel may contribute to those mechanical cues that eventually facilitated astrocytic differentiation. To test this hypothesis, we first examined the hydrogel morphology carefully using SEM at multiple time points, i.e., before, during, and after the differentiation. As expected, we observed an increasing rupture on the hydrogel surface with time (Fig. 6A). In particular, gel ruptures were observed at the cell-hydrogel interface

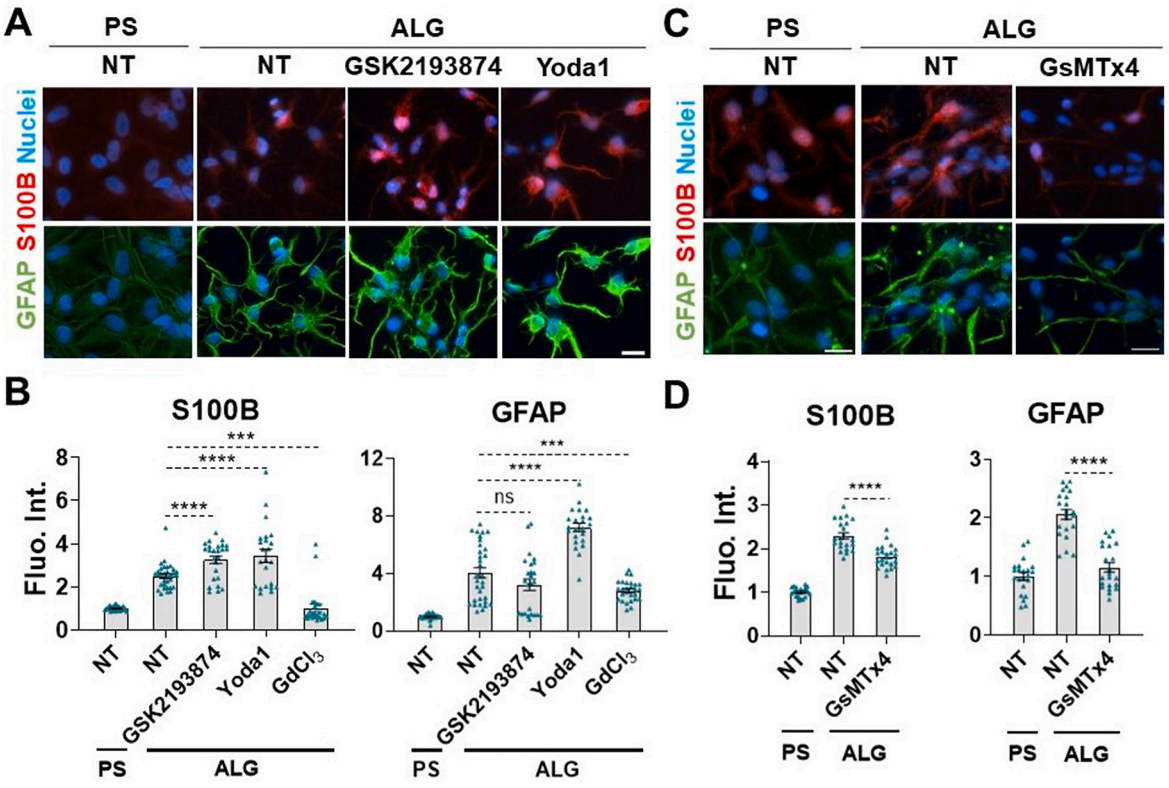

Fig. 4. Piezo1 but not TRPV4 contributes to promoting astrocytic differentiation on the hydrogel. **(A)** Immunofluorescence of S100B and GFAP after astrocytic differentiation under the conditions as indicated. **(B)** Quantifications on the immunofluorescence of S100B and GFAP as in (A). Data for $GdCl_3$ treatment are from Fig. 3F (column 2&3, reproduced for comparison). **(C)** Effect of GsMTx4 treatment on S100B and GFAP immunofluorescence after astrocytic differentiation. **(D)** Quantifications on S100B and GFAP immunofluorescence as in (C). Data are shown as averaged total cellular fluorescence intensity. N ≥ 21 imaging fields from three experiments. All data are presented as Mean ± SE, normalized to the first columns. NT, nontreated control. Ns, $p > 0.05$; **$p < 0.01$, ***$p < 0.001$, ****$p < 0.0001$, two-tailed student's *t*-test. (Scale bars: 20 μm).

after the differentiation (Fig. 6B, arrows). Further, we characterized the hydrogel elasticity before, during, and after the differentiation using AFM, and found that the gel became softer with time (Fig. 6C). This is interesting because the change in hydrogel elasticity has somehow mimicked that in brain during neurodegeneration, in which brain softening occurs [38,39]. The SEM and AFM characterizations showed that the hydrogel underwent a progressive rupture or breakdown during the astrocytic differentiation, accompanied by changes in mechanical properties. In addition, we measured the Ca^{2+} concentration in the tissue culture supernatant during the differentiation, and found that it kept increasing with time (Fig. 6D), suggesting a continuous release of Ca^{2+} from the hydrogel. This finding explains the possible reason of the gel decrosslinking and changes in mechanical properties, i.e., the Ca^{2+} ions that have crosslinked alginate are continuously exchanged by the nongelling ions from the medium, such as Na^{+}, resulting in subtle breakdown, rupture or swelling of the gel, and a decrease in elasticity. All these changes can serve as mechanical stimuli to the cells, and prompt the astrocytic differentiation.

To summarize, we conclude that a spontaneous, subtle, and progressive hydrogel decrosslinking can generate mechanical cues that are transmitted to the cells. These cues activate Piezo1 Ca^{2+} channel, facilitate actin cytoskeleton assembly, and eventually lead to promoted astrocytic differentiation through a YAP/TEAD-dependent transcriptional regulation on the alginate hydrogel (Fig. 6E).

4. Discussion and conclusion

In this work, we have demonstrated an alginate hydrogel-based platform that can significantly improve the astrocytic differentiation efficiency of hNSCs. *In vitro*, astrocytes are normally induced from NSCs or induced pluripotent stem cells (iPSCs). The traditional differentiation method from NSCs takes 1–3 weeks [4,5], and that from iPSCs is more time-consuming and complicated [40]. Alginate hydrogel is an excellent biomaterial for neural cell culture and differentiation, which has been shown to regulate astrocyte development and activities [41,42]. Here, our method using the alginate hydrogel as a substrate can largely shorten the time course for astrocytic differentiation. Moreover, the preparation of hydrogel is simple, requiring no complex fabrications, and the effect of the hydrogel in boosting astrocyte generation is highly reproducible. The obtained human astrocytes can be further characterized and employed in the future research of neurobiology.

Next, we have elucidated the underlying mechanism that leads to the enhanced astrocytic differentiation on the hydrogel from a mechanobiology perspective, and have revealed a novel regulatory pathway through the stretch-activated Ca^{2+} channels, actomyosin cytoskeleton, and YAP-mediated transcription. Earlier studies have demonstrated a BMP-induced astrocytic differentiation pathway facilitated by YAP and Smad-mediated transcription in rodents [10,11]. Our work shows that the YAP-TEAD interaction is necessary for promoting the serum-induced astrogenesis in the hNSCs; whether the YAP-Smad axis also makes contribution would be interesting to figure out in the future.

The Piezo1 activity, triggered by cytoskeletal traction force, has been shown to facilitate YAP nuclear translocation and transcription [9,36], consistent with our results. However, Piezo1 and YAP are indicated to suppress astrocytic development in one of those studies [9]. This contradiction can be due to the different substrates employed: while the mechanotransduction mechanism revealed in our work is based on the soft hydrogel substrate (elastic modulus ~ 1 kPa), the other is based on a conventional coverslip (elastic modulus in the order of GPa). The dominant regulatory pathway for astrocytic differentiation on stiff or

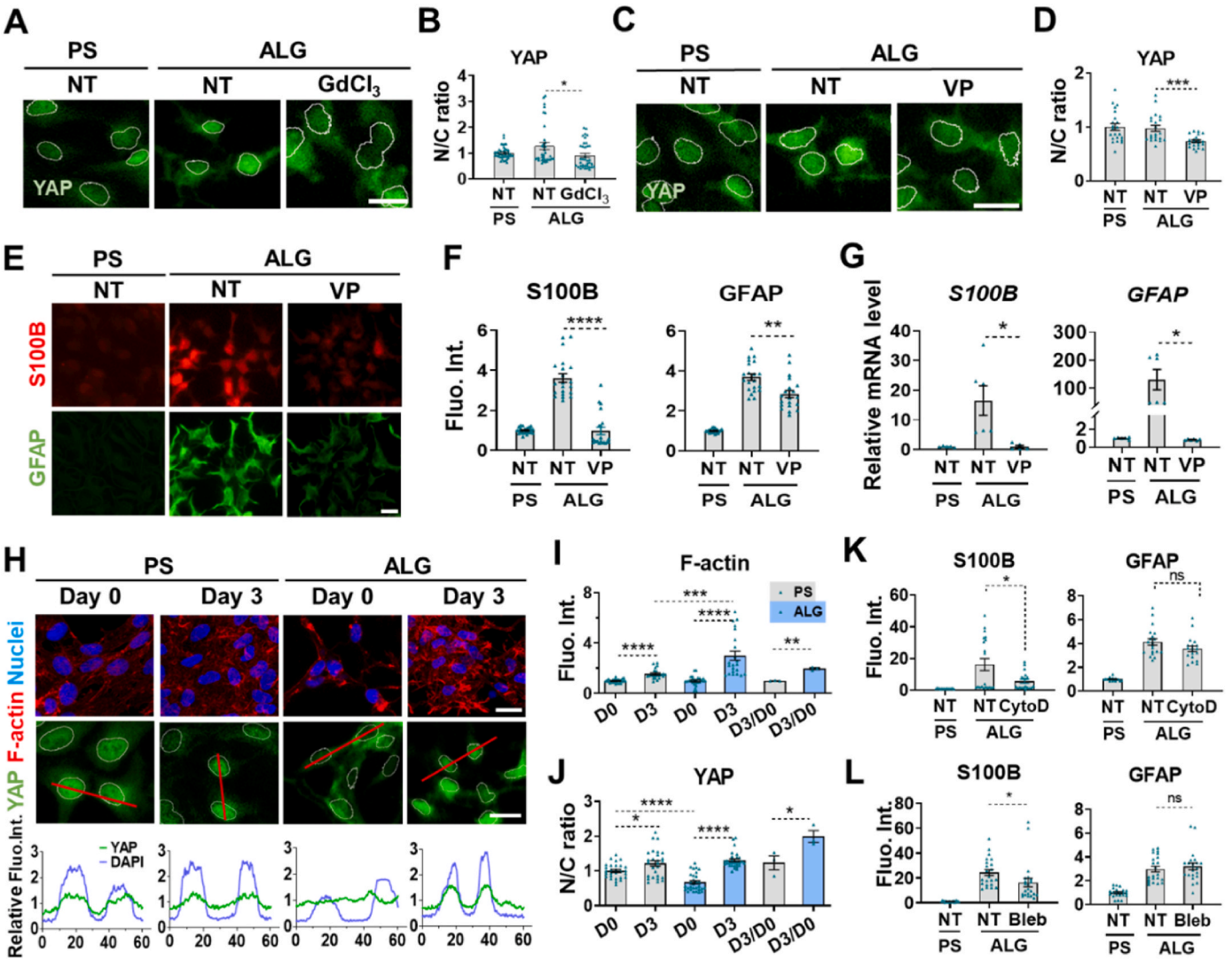

Fig. 5. The YAP-mediated transcription and actomyosin cytoskeleton contribute to astrocytic differentiation on the hydrogel. **(A)** YAP immunofluorescence indicating nuclear localization (circled by white lines) in cells grown on PS and on hydrogel without or with the treatment of $GdCl_3$. **(B)** Quantifications on YAP nuclear-to-cytoplasmic (N/C) ratio as in (A). N ≥ 36 imaging fields from three experiments. **(C)** YAP immunofluorescence in cells grown on PS and on hydrogel without or with the treatment of verteporfin (VP). **(D)** Quantifications on YAP N/C ratio as in (C). N ≥ 21 imaging fields from three experiments. **(E–F)** Immunofluorescence images (E) and quantifications (F) of the astrocytic markers S100B (red) and GFAP (green) in cells on PS and on hydrogel without or with the treatment of VP. N ≥ 20 imaging fields from three experiments. **(G)** Relative mRNA levels of astrocytic markers in cells differentiated on PS and on hydrogel without or with VP treatment. *GAPDH* gene was used as an internal control. N = 6 from two independent experiments. **(H)** (upper) Immunofluorescence of F-actin (red) and YAP (green) in cells grown on PS and alginate hydrogel (ALG) before (Day 0) and after (Day 3) astrocytic differentiation. Nuclei are stained by DAPI (blue) or circled by a white line. (lower) Intensity profiles of YAP and DAPI fluorescence along the red lines. Values are normalized to the average value of YAP intensity. **(I–J)** Quantification on F-actin intensity (I) and N/C ratio of YAP fluorescence (J) as in (H). N ≥ 22 imaging fields from three experiments. The Day3-to-Day0 ratios (D3/D0) are quantified by the mean value from three experiments. **(K–L)** Effects of Cytochalasin D (K) or Blebbistatin (L) treatment on astrocytic differentiation to cells on the hydrogel. Quantifications are based on immunofluorescence images. N ≥ 17 imaging fields from two experiments. "Fluo. Int." indicates averaged total cellular fluorescence intensity per image. All data are presented as Mean ± SE, normalized to the first columns. NT, nontreated control. Ns, $p > 0.05$; *$p < 0.05$, **$p < 0.01$, ***$p < 0.001$, ****$p < 0.0001$, two-tailed student's *t*-test. (Scale bars: 20 μm). (For interpretation of the references to color in this figure legend, the reader is referred to the Web version of this article.)

soft substrate may be distinct because of different cellular tension. The questions regarding how the Piezo1-mediated Ca^{2+} signaling is involved in the regulation of YAP translocation and how the YAP/TEAD-mediated transcription promotes the gene expression toward astrogenesis remain unclear, which requires further investigations.

Interestingly, it has been reported by several previous studies that the matrix degradation-induced cellular traction can regulate stem cell fate, using 3D hydrogels [43,44]. Unlike those works in which the hydrogel was degraded or digested by the embedded cells themselves, our study demonstrates a new finding in 2D, where the environmental "weathering effect" of the hydrogel plays a role in promoting cell differentiation. As this effect alters the mechanical properties of the hydrogel, in particular, resulting in hydrogel softening that recapitulates the softened brain in the context of neurodegeneration [38,39], our system may provide a simplified platform to study the mechanobiological mechanisms of neurodegenerative disorders [45].

Collectively, our study has shown that the alginate hydrogel can drastically promote the astrocytic differentiation of hNSCs through mechanical regulations via stretch-activated Ca^{2+} channels, actomyosin cytoskeleton and YAP-mediated transcription. While demonstrating an original and efficient approach to obtain astrocytes *in vitro*, we provide a practical biomaterial platform to study neuromechanobiology, and

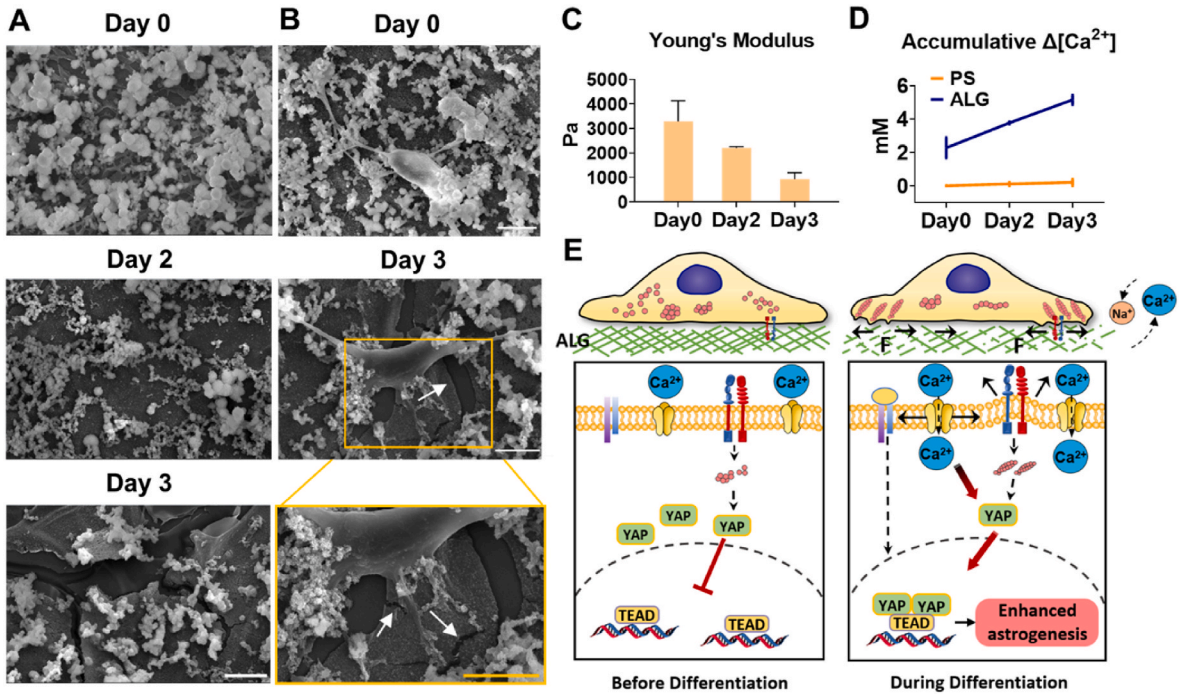

Fig. 6. The mechanotransduction mechanism of the enhanced astrocytic differentiation on the hydrogel. **(A)** SEM images showing the time-dependent rupture at the hydrogel surface. The alginate hydrogel had been incubated in a culture medium to mimic the differentiation condition before subjected to SEM imaging. **(B)** SEM images showing the cell-hydrogel interface before (Day 0) and after (Day 3) the differentiation. The yellow window is zoomed-in, and the arrows indicate hydrogel ruptures at the cell interface. **(C)** Variation in the alginate hydrogel elasticity during the astrocytic differentiation, characterized by AFM. N = 3. **(D)** The Ca^{2+} concentration that increased in the tissue culture supernatant ($\Delta[Ca^{2+}]$, compared to blank medium) in the cultures using PS or alginate hydrogel as a substrate. Data are shown as accumulative $[Ca^{2+}]$ increase with time. N = 2. **(E)** Model interpreting the mechanotransduction mechanism of the enhanced astrogenesis on alginate hydrogel. Before the differentiation, the soft hydrogel restricts YAP nuclear translocation and transcription. During the differentiation, decrosslinking or subtle breakdown of the hydrogel continuously occurs, transmitting mechanical forces to the cells, which promotes mechanosensitive Ca^{2+} channels activation and actin polymerization that facilitates YAP nuclear translocation and transcription, resulting in elevated astrocytic gene expression. Data are presented as Mean ± SE. (Scale bars: 20 μm). (For interpretation of the references to color in this figure legend, the reader is referred to the Web version of this article.)

offers novel insights into the mechanism of astrocyte development from a lens of mechanobiology.

CRediT authorship contribution statement

Zhongqian Liu: Methodology, Validation, Formal analysis, Investigation, Data curation, Writing – original draft, Visualization, Project administration. **Shijie Mao:** Investigation. **Yubin Hu:** Resources. **Feng Liu:** Writing – review & editing, Supervision. **Xiaowei Shao:** Conceptualization, Writing – original draft, Writing – review & editing, Visualization, Supervision, Project administration, Funding acquisition.

Declaration of competing interest

The authors declare that they have no known competing financial interests or personal relationships that could have appeared to influence the work reported in this paper.

Data availability

Data will be made available on request.

Acknowledgements

We thank Prof. Lin Han and Prof. Yu Zhang from Institute of Marine Science and Technology of Shandong University for their generous sharing of resources and valuable suggestions on this project. We thank Prof. Zhaocun Shen and Prof. Kunyan Sui from Qingdao University for their kind assistance in rheological measurement and analysis. We thank Chao Wang and Ping Li from Institute of Marine Science and Technology of Shandong University for the guidance in fluorescence microscopy and electron microscopy. We thank Haiyan Yu, Xiaomin Zhao, Yuyu Guo, and Sen Wang from Core Facilities for Life and Environmental Sciences of SKLMT (State Key Laboratory of Microbial Technology, Shandong University) for assistance in confocal microscopy and SEM. We thank Shuqiang Xu from Institute of Cultural Heritage of Shandong University for assistance in SEM imaging and analysis. This work is supported by the National Natural Science Foundation of China (Grant No. 32000887), the Natural Science Foundation of Jiangsu Province (Grant No. BK20200222), and the Shandong University Foundation for Future Scholar Plan.

Appendix A. Supplementary data

Supplementary data to this article can be found online at https://doi.org/10.1016/j.mtbio.2023.100735.

References

[1] S.A. Liddelow, M.V. Sofroniew, Astrocytes usurp neurons as a disease focus, Nat. Neurosci. 22 (2019) 512–513, https://doi.org/10.1038/s41593-019-0367-6.
[2] L. Maiolo, V. Guarino, E. Saracino, A. Convertino, M. Melucci, M. Muccini, L. Ambrosio, R. Zamboni, V. Benfenati, Glial interfaces: advanced materials and devices to uncover the role of astroglial cells in brain function and dysfunction, Advanced healthcare materials 10 (2021), e2001268, https://doi.org/10.1002/adhm.202001268.
[3] X. Yu, J. Nagai, B.S. Khakh, Improved tools to study astrocytes, Nat. Rev. Neurosci. 21 (2020) 121–138, https://doi.org/10.1038/s41583-020-0264-8.
[4] Y. Sun, S. Pollard, L. Conti, M. Toselli, G. Biella, G. Parkin, L. Willatt, A. Falk, E. Cattaneo, A. Smith, Long-term tripotent differentiation capacity of human neural stem (ns) cells in adherent culture, Mol. Cell. Neurosci. 38 (2008) 245–258, https://doi.org/10.1016/j.mcn.2008.02.014.

[5] M. Magistri, N. Khoury, E.M. Mazza, D. Velmeshev, J.K. Lee, S. Bicciato, P. Tsoulfas, M.A. Faghihi, A comparative transcriptomic analysis of astrocytes differentiation from human neural progenitor cells, Eur. J. Neurosci. 44 (2016) 2858–2870, https://doi.org/10.1111/ejn.13382.
[6] R.D. Bierman-Duquette, G. Safarians, J. Huang, B. Rajput, J.Y. Chen, Z.Z. Wang, S. K. Seidlits, Engineering tissues of the central nervous system: interfacing conductive biomaterials with neural stem/progenitor cells, Adv Healthc Mater 11 (2022), e2101577, https://doi.org/10.1002/adhm.202101577.
[7] N.D. Leipzig, M.S. Shoichet, The effect of substrate stiffness on adult neural stem cell behavior, Biomaterials 30 (2009) 6867–6878, https://doi.org/10.1016/j.biomaterials.2009.09.002.
[8] H. Oyama, A. Nukuda, S. Ishihara, H. Haga, Soft surfaces promote astrocytic differentiation of mouse embryonic neural stem cells via dephosphorylation of mrlc in the absence of serum, Sci. Rep. 11 (2021), 19574, https://doi.org/10.1038/s41598-021-99059-5.
[9] M.M. Pathak, J.L. Nourse, T. Tran, J. Hwe, J. Arulmoli, D.T.T. Le, E. Bernardis, L. A. Flanagan, F. Tombola, Stretch-activated ion channel piezo1 directs lineage choice in human neural stem cells, Proc. Natl. Acad. Sci. U.S.A. 111 (2014) 16148–16153, https://doi.org/10.1073/pnas.1409802111.
[10] Z. Huang, J. Hu, J. Pan, Y. Wang, G. Hu, J. Zhou, L. Mei, W.C. Xiong, Yap stabilizes smad1 and promotes bmp2-induced neocortical astrocytic differentiation, Development 143 (2016) 2398–2409, https://doi.org/10.1242/dev.130658.
[11] Z. Huang, D. Sun, J.X. Hu, F.L. Tang, D.H. Lee, Y. Wang, G. Hu, X.J. Zhu, J. Zhou, L. Mei, W.C. Xiong, Neogenin promotes bmp2 activation of yap and smad1 and enhances astrocytic differentiation in developing mouse neocortex, J. Neurosci. 36 (2016) 5833–5849, https://doi.org/10.1523/JNEUROSCI.4487-15.2016.
[12] S. Rammensee, M.S. Kang, K. Georgiou, S. Kumar, D.V. Schaffer, Dynamics of mechanosensitive neural stem cell differentiation, Stem Cell. 35 (2017) 497–506, https://doi.org/10.1002/stem.2489.
[13] P.H. Kang, D.V. Schaffer, S. Kumar, Angiomotin links rock and yap signaling in mechanosensitive differentiation of neural stem cells, Mol. Biol. Cell 31 (2020) 386–396, https://doi.org/10.1091/mbc.E19-11-0602.
[14] L. Li, J. Eyckmans, C.S. Chen, Designer biomaterials for mechanobiology, Nat. Mater. 16 (2017) 1164–1168, https://doi.org/10.1038/nmat5049.
[15] B. Ozkale, M.S. Sakar, D.J. Mooney, Active biomaterials for mechanobiology, Biomaterials 267 (2021), 120497, https://doi.org/10.1016/j.biomaterials.2020.120497.
[16] D.J. Hadley, E.A. Silva, Thaw-induced gelation of alginate hydrogels for versatile delivery of therapeutics, Ann. Biomed. Eng. 47 (2019) 1701–1710, https://doi.org/10.1007/s10439-019-02282-5.
[17] A. Tabet, S. Mommer, J.A. Vigil, C. Hallou, H. Bulstrode, O.A. Scherman, Mechanical characterization of human brain tissue and soft dynamic gels exhibiting electromechanical neuro-mimicry, Adv. Healthc. Mater. 8 (2019), e1900068, https://doi.org/10.1002/adhm.201900068.
[18] A.E. Forte, S.M. Gentleman, D. Dini, On the characterization of the heterogeneous mechanical response of human brain tissue, Biomech. Model. Mechanobiol. 16 (2017) 907–920, https://doi.org/10.1007/s10237-016-0860-8.
[19] C.W. Macosko, Rheology: Principles, Measurements, and Applications, first ed., Wiley VCH, 1996.
[20] D.E. Discher, P. Janmey, Y.L. Wang, Tissue cells feel and respond to the stiffness of their substrate, Science 310 (2005) 1139–1143, https://doi.org/10.1126/science.1116995.
[21] N. Nisenholz, K. Rajendran, Q. Dang, H. Chen, R. Kemkemer, R. Krishnan, A. Zemel, Active mechanics and dynamics of cell spreading on elastic substrates, Soft Matter 10 (2014) 7234–7246, https://doi.org/10.1039/c4sm00780h.
[22] S. Li, H. Bai, X. Chen, S. Gong, J. Xiao, D. Li, L. Li, Y. Jiang, T. Li, X. Qin, H. Yang, C. Wu, F. You, Y. Liu, Soft substrate promotes osteosarcoma cell self-renewal, differentiation, and drug resistance through mir-29b and its target protein spin 1, ACS Biomater. Sci. Eng. 6 (2020) 5588–5598, https://doi.org/10.1021/acsbiomaterials.0c00816.
[23] X. Shao, C. Wang, C. Wang, L. Han, Y. Han, D. Nižetić, Y. Zhang, L. Han, Mechanical stress induces a transient suppression of cytokine secretion in astrocytes assessed at the single-cell level with a high-throughput microfluidic chip, Adv Healthc Mater 10 (2021), e2100698, https://doi.org/10.1002/adhm.202100698.
[24] C. Yang, M.W. Tibbitt, L. Basta, K.S. Anseth, Mechanical memory and dosing influence stem cell fate, Nat. Mater. 13 (2014) 645–652, https://doi.org/10.1038/nmat3889.
[25] D. Tran, R. Galletti, E.D. Neumann, A. Dubois, R. Sharif-Naeini, A. Geitmann, J. M. Frachisse, O. Hamant, G.C. Ingram, A mechanosensitive ca(2+) channel activity is dependent on the developmental regulator dek1, Nat. Commun. 8 (2017) 1009, https://doi.org/10.1038/s41467-017-00878-w.
[26] H. Reyes-Pardo, D.P. Sanchez-Herrera, Mechanosensitive ion channel inhibitors promote the stiffening of the plasma membrane of mouse sensory neurons, Soft Matter 15 (2019) 8320–8328, https://doi.org/10.1039/c9sm01230c.
[27] C.K. Thodeti, B. Matthews, A. Ravi, A. Mammoto, K. Ghosh, A.L. Bracha, D. E. Ingber, Trpv4 channels mediate cyclic strain–induced endothelial cell reorientation through integrin-to-integrin signaling, Circ. Res. 104 (2009) 1123–1130, https://doi.org/10.1161/CIRCRESAHA.108.192930.
[28] C.J. O'Conor, H.A. Leddy, H.C. Benefield, W.B. Liedtke, F. Guilak, Trpv4-mediated mechanotransduction regulates the metabolic response of chondrocytes to dynamic loading, Proc. Natl. Acad. Sci. USA 111 (2014) 1316–1321, https://doi.org/10.1073/pnas.1319569111.
[29] W.M. Botello-Smith, W. Jiang, H. Zhang, A.D. Ozkan, Y.C. Lin, C.N. Pham, J. J. Lacroix, Y. Luo, A mechanism for the activation of the mechanosensitive piezo1 channel by the small molecule yoda1, Nat. Commun. 10 (2019) 4503, https://doi.org/10.1038/s41467-019-12501-1.
[30] C. Bae, F. Sachs, P.A. Gottlieb, The mechanosensitive ion channel piezo1 is inhibited by the peptide gsmtx4, Biochemistry 50 (2011) 6295–6300, https://doi.org/10.1021/bi200770q.
[31] P.A. Gottlieb, T. Barone, F. Sachs, R. Plunkett, Neurite outgrowth from pc12 cells is enhanced by an inhibitor of mechanical channels, Neurosci. Lett. 481 (2010) 115–119, https://doi.org/10.1016/j.neulet.2010.06.066.
[32] D. Han, M. Kwon, S.M. Lee, S.J. Pleasure, K. Yoon, Non-cell autonomous promotion of astrogenesis at late embryonic stages by constitutive yap activation, Sci. Rep. 10 (2020) 7041, https://doi.org/10.1038/s41598-020-63890-z.
[33] Y. Guo, Z. Zhu, Z. Huang, L. Cui, W. Yu, W. Hong, Z. Zhou, P. Du, C.Y. Liu, Ck2-induced cooperation of hhex with the yap-tead4 complex promotes colorectal tumorigenesis, Nat. Commun. 13 (2022) 4995, https://doi.org/10.1038/s41467-022-32674-6.
[34] L. Hu, Y. Sun, S. Liu, H. Erb, A. Singh, J. Mao, X. Luo, X. Wu, Discovery of a new class of reversible tea domain transcription factor inhibitors with a novel binding mode, Elife 11 (2022), https://doi.org/10.7554/eLife.80210.
[35] J. Ye, T.S. Li, G. Xu, Y.M. Zhao, N.P. Zhang, J. Fan, J. Wu, Jcad promotes progression of nonalcoholic steatohepatitis to liver cancer by inhibiting lats2 kinase activity, Cancer Res. 77 (2017) 5287–5300, https://doi.org/10.1158/0008-5472.CAN-17-0229.
[36] B. Zhu, W. Qian, C. Han, T. Bai, X. Hou, Piezo 1 activation facilitates cholangiocarcinoma metastasis via hippo/yap signaling axis, Mol. Ther. Nucleic Acids 24 (2021) 241–252, https://doi.org/10.1016/j.omtn.2021.02.026.
[37] S. Dupont, L. Morsut, M. Aragona, E. Enzo, S. Giulitti, M. Cordenonsi, F. Zanconato, J. Le Digabel, M. Forcato, S. Bicciato, N. Elvassore, S. Piccolo, Role of yap/taz in mechanotransduction, Nature 474 (2011) 179–183, https://doi.org/10.1038/nature10137.
[38] G. McIlvain, J.M. Schneider, M.A. Matyi, M.D. McGarry, Z. Qi, J.M. Spielberg, C. L. Johnson, Mapping brain mechanical property maturation from childhood to adulthood, Neuroimage 263 (2022), 119590, https://doi.org/10.1016/j.neuroimage.2022.119590.
[39] L.V. Hiscox, H. Schwarb, M.D.J. McGarry, C.L. Johnson, Aging brain mechanics: progress and promise of magnetic resonance elastography, Neuroimage 232 (2021), 117889, https://doi.org/10.1016/j.neuroimage.2021.117889.
[40] J. Tcw, M. Wang, A.A. Pimenova, K.R. Bowles, B.J. Hartley, E. Lacin, S.I. Machlovi, R. Abdelaal, C.M. Karch, H. Phatnani, P.A. Slesinger, B. Zhang, A.M. Goate, K. J. Brennand, An efficient platform for astrocyte differentiation from human induced pluripotent stem cells, Stem Cell Rep. 9 (2017) 600–614, https://doi.org/10.1016/j.stemcr.2017.06.018.
[41] Y. Hu, G. Huang, J. Tian, J. Qiu, Y. Jia, D. Feng, Z. Wei, S. Li, F. Xu, Matrix stiffness changes affect astrocyte phenotype in an in vitro injury model, NPG Asia Mater. 13 (2021) 35, https://doi.org/10.1038/s41427-021-00304-0.
[42] C.M. Tringides, M. Boulingre, A. Khalil, T. Lungjangwa, R. Jaenisch, D.J. Mooney, Tunable conductive hydrogel scaffolds for neural cell differentiation, Adv Healthc Mater 12 (2023), e2202221, https://doi.org/10.1002/adhm.202202221.
[43] S. Khetan, M. Guvendiren, W.R. Legant, D.M. Cohen, C.S. Chen, J.A. Burdick, Degradation-mediated cellular traction directs stem cell fate in covalently crosslinked three-dimensional hydrogels, Nat. Mater. 12 (2013) 458–465, https://doi.org/10.1038/nmat3586.
[44] C.M. Madl, B.L. LeSavage, R.E. Dewi, K.J. Lampe, S.C. Heilshorn, Matrix remodeling enhances the differentiation capacity of neural progenitor cells in 3d hydrogels, Adv. Sci. 6 (2019), 1801716, https://doi.org/10.1002/advs.201801716.
[45] X. Shao, Z. Liu, S. Mao, L. Han, Unraveling the mechanobiology underlying traumatic brain injury with advanced technologies and biomaterials, Adv Healthc Mater 11 (2022), e2200760, https://doi.org/10.1002/adhm.202200760.